Supercond. Sci. Technol. 11 (1998) 1241–1250. Printed in the UK PII: S0953-2048(98)93547-3

Simulation of magnetic relaxation measurements of tetragonal $Bi_2Sr_2CaCu_2O_{8+x}$ and $Bi_2Sr_2Ca_2Cu_3O_{10+y}$ thin films

M Holiastou†, M Pissas†, D Niarchos†, P Haibach‡, U Frey‡ and H Adrian‡

† IMS, NCSR 'Demokritos', 15310 Athens, Greece
‡ Johanness Gutenberg Universitat, 55099 Mainz, Germany

Received 15 April 1998

Abstract. Magnetic relaxation data at various temperatures and magnetic fields are taken from high-quality, epitaxial thin films of $Bi_2Sr_2CaCu_2O_{8+x}$ and $Bi_2Sr_2Ca_2Cu_3O_{10+y}$ and are simulated using a method developed by Brandt and coworkers. Assuming thermally activated resistivity $\rho(j) = \rho_0\, e^{-U(j)/kT}$ and logarithmic activation energy $U(j) = U_c \ln(j_c/j)$ we obtain good simulations of the experimental data. The critical current resulting from the simulation is evaluated as a function of the temperature and is found to decrease linearly with it and the current–voltage characteristics are extracted and are linear on a $\log E$–$\log j$ scale at all temperatures. The activation energy is calculated as a function of the current and it is shown to be a decreasing function of the magnetic field following a power law $B^{-\alpha}$. The critical current is also shown to decrease with the magnetic field and can be described well by the exponential form e^{-B/B_0}. Comparison between the two phases $Bi_2Sr_2CaCu_2O_{8+x}$ and $Bi_2Sr_2Ca_2Cu_3O_{10+y}$ indicates that pinning in the $Bi_2Sr_2Ca_2Cu_3O_{10+y}$ film is stronger due to the lower anisotropy of this phase and probably because of the existence of more defects. Finally, the distribution of the local magnetic moment and the magnetic induction on the surface of the film at different times during the relaxation procedure is nicely depicted with surface and contour plots.

1. Introduction

One of the basic features that the high-temperature superconductors exhibit is the thermally activated motion of the vortex system. Because of the small coherence length and large anisotropy of these materials, the pinning of vortices is weak causing, at the elevated temperatures available in the experiment, any current, screening or transport, to decay in time. This decay can be observed directly in magnetic relaxation experiments, where a magnetic field is applied to the superconductor and its magnetic moment is recorded as a function of time. Such measurements are most commonly used for the determination of several properties of superconductors such as the pinning potential, critical current or current voltage characteristics, which are extracted from the decay rate of the current.

The response of a superconductor to the application of a magnetic field is by no means a trivial problem and various models have been constructed to describe it. However, many of those adopt simplifications, such as homogeneous current distributions or constant critical currents [1–4]. More recent work solves the problem analytically for the idealized geometry of circular disks and long strips [5, 6]. In 1995 the problem was solved numerically by Brandt and coworkers for the realistic situation of a thin rectangular superconductor in an applied field varying with time [7, 8]. In the work of Brandt [7] and Schuster *et al* [8] it is shown that the Maxwell equations lead to an equation of motion for the current of the superconductor. This equation can be solved numerically on a personal computer and consequently the electromagnetic properties of the superconductor can be calculated. In this work, we take advantage of this latest progress to simulate the magnetic moment of superconducting thin films using no simplifications, but taking into account the exact film geometry, the external field's variation with time and all space dependences. More specifically, we measure the magnetic moment of $Bi_2Sr_2CaCu_2O_{8+x}$ and $Bi_2Sr_2Ca_2Cu_3O_{10+y}$ superconducting thin films as a function of time and simulate it using the method mentioned above and adopting a thermally activated law for the resistivity ($\rho(j) = \rho_0 \, e^{-U(j)/kT}$) and a logarithmic law for the potential energy ($U(j) = U_c \ln(j_c/j)$).

This work is organized as follows. In section 2, we give the basic characteristics on the film preparation and properties as well as details of the relaxation measurements. In section 3, we discuss the basic assumptions made for the resistivity and the activation energy and describe the computational procedure. In section 4, we present the results of the simulation, i.e. the calculated magnetization curves and the corresponding values of the fitting parameters, and discuss them. For the reader who is unfamiliar with the method of Brandt and his coworkers, which is fully described in several papers [7–10], we give an outline in the appendix. There, we support the various assumptions of the method when applied to a rectangular thin film and also derive the Fourier transformation of the final equation of motion, which is the one we integrate computatively in this work, instead of the corresponding equation in direct space that Schuster *et al* use in their original publication [8].

2. Experimental details

Superconducting thin films of $Bi_2Sr_2CaCu_2O_{8+x}$ (Bi-2212) and $Bi_2Sr_2Ca_2Cu_3O_{10+y}$ (Bi-2223) are prepared by DC sputtering. The Bi-2212 and Bi-2223 films are deposited from $Bi_{2.05}Sr_2CaCu_2O_{8+x}$ and $Bi_{2.05}Sr_2Ca_2Cu_{3.3}O_{10+y}$ targets respectively, on $SrTiO_3$ (100) substrates, at 830 °C substrate temperature and 3 mbar pressure of pure oxygen. Details of the experimental conditions can be found in [11].

The films are single phase and have their c-axis normal to the film surface, as was revealed by x-ray θ–2θ scans [11]. In addition, the films are fully epitaxial, which was checked by extensive single-crystal diffraction measurements [11] and confirmed by polarized micro Raman spectroscopy [12]. The Bi-2212 thin film has an onset for superconductivity at $T_c^{onset} = 88$ K and a transition width of ΔT_c $(= T_c^{90\%} - T_c^{10\%}) = 5$ K and the Bi-2223 thin film has onset at $T_c^{onset} = 84$ K and a transition width of ΔT_c $(= T_c^{90\%} - T_c^{10\%}) = 3$ K, measured by the AC susceptibility technique [11]. The films are square with sides 0.50 cm (Bi-2212 film) and 0.46 cm (Bi-2223 film) and thickness approximately 1000 Å, estimated from the deposition rate during preparation.

The relaxation experiments are performed with a commercial SQUID magnetometer (Quantum Design MPMS2) with the applied magnetic field normal to the film surface and a scan length of 2 cm, so as to ensure field homogeneity. The relaxation data are collected in a field-on mode in the following way. First, the film is zero-field cooled at the desired temperature. The external field is then applied and, as soon as it reaches the desired value, the data start being collected. Special care has been taken concerning the field application, which must be made monotonically towards the final value, an essential point for samples with hysteretic behaviour. One set of measurements covers a temperature range from 5 K to 60 K and is performed for each temperature with the least magnetic field sufficient to cause full flux penetration into the sample. The latter is evaluated from magnetic hysteresis loop data taken from the same films [13] as 1.5 times the field at which the magnetic moment acquires a maximum. To detect magnetic field dependences of the various quantities, a set of relaxation data is taken at fields 500 G $\le H_\alpha \le$ 40 kG and temperatures $T = 5$ K for the two films. All the experimental values of temperature and magnetic field are listed in table 1.

In figure 1(a) a representative set of experimental data at temperatures $T = 5$, 10, 20, 30, 40, 50 and 60 K and magnetic fields $H_\alpha = 500$, 500, 300, 200, 80, 80 and 20 G respectively (the smallest values ensuring full flux penetration) are shown (square symbols) for the Bi-2223 thin film on a semilogarithmic plot. It can be seen that the plots are linear in $\log t$ at large times. At higher temperatures the observed magnetic moment decreases and this is due primarily to the critical current being smaller and secondly to the relaxation being faster as a result of the increase in thermal energy. The data for the Bi-2212 thin film are similar and at small temperatures are characterized by larger absolute values of the magnetic moment as the size of the Bi-2212 film is slightly larger, but as the temperature grows the Bi-2212 data curve gradually crosses above the Bi-2223 curve because the relaxation rate for the Bi-2223 film is lower. This can be seen in figure 1(b), where data for the two films at the common temperature and field values of $T = 30$ K and $H = 200$ G are plotted. The slope of the Bi-2223 curve is obviously smaller and this holds for all temperatures and fields. The slower relaxation of the Bi-2223 thin film is an indication of stronger pinning in this phase and this will be verified below, from the larger values of the simulation parameter U_c, which determines the slope of the curve.

3. Computational procedure

All the relaxation measurements are simulated using a method as described by Brandt and his coworkers, which we outline in the appendix. As it is described there, the magnetic moment of the thin rectangular film can be calculated if we solve the following equation of motion (equation (A15)):

$$\dot{g}_K(t) = \iint_{\substack{surface\\ of\ film}} Q^{-1}(\boldsymbol{r}, \boldsymbol{r}') \left(\frac{1}{ab}\right)^{1/2} \sin(K_x x) \sin(K_y y) \times \left\{ c \nabla' \cdot \left[\frac{\rho}{d} \nabla' g(\boldsymbol{r}', t) \right] - \dot{H}_\alpha(t) \right\} \mathrm{d}^2 r' \, \mathrm{d}^2 r.$$

$g_K(t)$ is the Fourier transform of the local magnetic moment $g(\boldsymbol{r}, t)$ which, when integrated over the film surface, gives the magnetic moment of the film versus the time. Notice that for the derivation of equation (A15) no assumptions have been made, other than the current flow being parallel to the film surface. This is justified by the film's c-axis orientation and the epitaxial properties ensure that the currents, running on the Cu–O planes (as a result of the external magnetic field applied normal to the surface), are parallel to the surface.

The properties of the films are taken into account by assuming for the resistivity the thermally activated form [14]

$$\rho = \rho_0 \, e^{-U(j)/kT} \tag{1}$$

Table 1. Values of the simulation parameters ρ_0, U_c, j_{c0}, B_0 for the $Bi_2Sr_2CaCu_2O_6$ and $Bi_2Sr_2Ca_2Cu_3O_8$ films corresponding to the experimental data at temperatures T and magnetic fields H_α and corresponding values of the simulation exponent n and the values $m(0)$ of the fitting parameters of the magnetization data at large times.

T (K)	H_α (G)	ρ_0 ($\mu\Omega$ cm)	U_c (K)	j_{c0} (10^5 A cm^{-2})	B_0 (G)	n (=U_c/kT)	$m(0)$ (emu)
Bi-2212							
5	500	1×10^{-8}	350	80.7	∞	70	−0.233
10	500	1×10^{-8}	550	73.0	∞	55	−0.214
20	300	1×10^{-8}	540	58.2	∞	27	−0.162
30	200	1×10^{-8}	660	38.0	∞	22	−0.105
40	80	1×10^{-8}	720	24.0	∞	18	−0.063
50	80	1×10^{-8}	500	17.3	∞	10	−0.035
60	20	1×10^{-8}	550	8.1	∞	9.2	−0.015
Bi-2223							
5	500	1×10^{-8}	400	96.8	∞	80	−0.215
10	500	1×10^{-8}	650	86.7	∞	65	−0.180
20	300	1×10^{-8}	600	70.5	∞	30	−0.150
30	200	1×10^{-8}	780	48.6	∞	19.5	−0.105
40	80	1×10^{-8}	740	33.1	∞	14.8	−0.066
50	80	1×10^{-8}	600	20.1	∞	12	−0.037
60	20	1×10^{-8}	660	8.3	∞	11	−0.011
Bi-2212							
5	500	1×10^{-8}	350	80.7	∞	70	−0.233
5	1000	1×10^{-8}	300	80.3	∞	60	−0.232
5	5000	1×10^{-8}	180	61.2	∞	36	−0.180
5	10 000	1×10^{-8}	150	40.2	∞	30	−0.114
5	20 000	1×10^{-7}	140	27.0	∞	28	−0.085
5	30 000	1×10^{-7}	130	21.6	∞	26	−0.070
5	40 000	1×10^{-7}	120	18.4	∞	24	−0.058
Bi-2223							
5	500	1×10^{-8}	400	96.8	∞	80	−0.215
5	1000	1×10^{-8}	350	94.7	∞	70	−0.205
5	5000	1×10^{-7}	220	76.4	∞	44	−0.160
5	10 000	1×10^{-7}	155	50.0	∞	31	−0.104
5	20 000	1×10^{-7}	130	33.4	∞	26	−0.077
5	30 000	1×10^{-7}	110	15.0	∞	22	−0.035
5	40 000	1×10^{-7}	120	12.9	∞	24	−0.027

where

$$U(j) = U_c \ln\left(\frac{j_c}{j}\right) \tag{2}$$

and

$$j_c = j_{c0}\, e^{-B/B_0}. \tag{3}$$

Equations (1) and (2) are equivalent to a power law $\rho = \rho_0 (j/j_c)^n$ for the resistivity, with $n = U_c/kT$. This power law, which is suggested by many authors [9, 10] offers the flexibility, by choosing the exponent n, to describe different regimes of film behaviour. For $n = 0$, the equation $\rho = \rho_0 (j/j_c)^n$ gives $\rho = \rho_0$, independent of j, which is the ohmic case realized for example in the flux-flow (FF) regime of unpinned vortices at high temperatures or high fields. $n = \infty$ implies that $j = 0$ or $j = j_c$ (since ρ must be finite), which means that the current, if it exists, is always equal to the critical current and it is the Bean behaviour of rigid pinning [1]. For $0 < n < \infty$, i.e. between the above-mentioned limits, there is the regime of flux creep to which our relaxation data correspond. This is confirmed by the results of the simulation that are $9 \leq n \leq 80$, depending on the temperature.

For the activation energy $U(j)$ there exist several models. In the Anderson–Kim model [15] U vanishes linearly with j: $U = U_c(1 - j/j_{c0})$. In the collective-creep model [16], $U = U_c[(j_{c0}/j)^\mu - 1]$ for $j \ll j_c$ while in a single-vortex pinning regime at low currents $U(j) = U_c \ln(j_c/j)$ [17]. The latter logarithmic form gives, as we find, very good simulation results and we adopt it in all measurements. It has been proposed by Zeldov *et al* [18], on the basis of current–voltage characteristics, and has since been used by many authors for the interpretation of magnetic relaxation results [19], magnetization hysteresis curves [20] or Hall-probe relaxation measurements [21]. The logarithmic barrier is close to a power law $(j_c/j)^\mu$ with $\mu \approx 1/7$ [22], which describes single-vortex pinning within the collective creep model. This is justified in our case, at least in small magnetic fields, since the critical current of the BSCCO thin films is at least $j_c \approx 10^6$ A cm^{-2}, as can be deduced from hysteresis loop data if we use the approximate relation $j_c = 3cm/\pi R^3 d$ with m the maximum magnetic moment of the loop. Consequently, the transverse correlation length of the flux lattice $R_c = \alpha_0(\xi/8\pi\lambda^2\mu_0)^{1/2}(B/j_c)^{1/2}$ [23, 24] is approximately equal to $0.1\alpha_0$, for $\xi \approx 30$ Å and $B = 500$ G, i.e. it is much lower than the intervortex spacing α_0. Thus, the vortex system is in the single-vortex pinning regime at low fields. In fact, it can be argued that it is in a single-pancake pinning

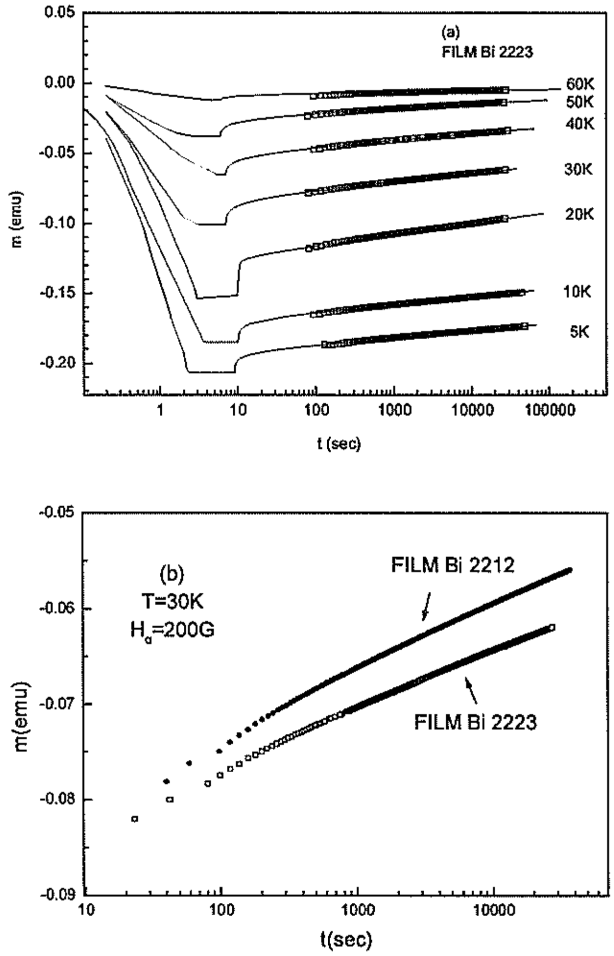

Figure 1. (*a*) Magnetic relaxation data at temperatures $T = 5$, 10, 20, 30, 40, 50 and 60 K and magnetic fields $H = 500$, 500, 300, 200, 80, 80 and 20 G respectively and the corresponding simulation curves for the $Bi_2Sr_2Ca_2Cu_3O_{8+y}$ thin film. (*b*) Magnetic relaxation data for the films $Bi_2Sr_2CaCu_2O_{6+x}$ and $Bi_2Sr_2Ca_2Cu_3O_{8+y}$ at the same temperature and magnetic field ($T = 30$ K and $H_{ext} = 80$ G).

regime, since the longitudinal correlation length is [25] $L_c = \varepsilon\xi(c\Phi_0/12\sqrt{3}\pi^2\lambda^2\xi j_c)^{1/2} \approx 2$ Å and thus smaller than the interlayer distance, which is ≈15 Å.

For the critical current we adopt the exponential law (3), which has often been used to take into account its decrease with the magnetic field [26, 27]. In that equation j_{c0} is the critical current in zero field ($B = 0$) and reflects the current-carrying capacity of the superconductor and B_0 is a phenomenological parameter related to the pinning ability: the smaller it is, the more drastic is the decrease of the critical current with field. Another possible decay law would be the Kim-like expression $j_c = j_{c0}/(1 + B/B_0)$ [28, 29], which has also been used by other groups [30, 31]. However, it turns out for a relaxation procedure that it makes no difference whether we use equation (3) or not and the reason is that the decrease of the magnetic field in the film during the time is too small to have an effect on the critical current. Thus we use equation (3) with $B_0 = \infty$, in other words $j_c = j_{c0}$ (=constant during the relaxation) and we keep in mind that the resulting simulation values of j_{c0} do not represent the critical current in zero field but the critical current at the field of the measurement. It must be noted, however, that this assumption would not be appropriate for simulations of experiments in which the magnetic field changes significantly, for example in magnetic hysteresis loops.

For the applied magnetic field rate $\dot{H}_\alpha(t)$ we assume a linear increase, i.e. $\dot{H}_\alpha(t) = H_\alpha/\Delta t$, where H_α is the applied field and Δt is the actual experimental time that it took for the SQUID magnetometer to apply it. We mentioned before that the application of the magnetic field is done monotonically as is required for samples with hysteretic behaviour. However, the value of the rate $\dot{H}_\alpha(t)$ may vary during the ramping. Still, if we consider that the actual values of Δt are of the order of seconds it can be understood that the specific form of $\dot{H}_\alpha(t)$ is not important and the above linear increase will be perfectly satisfactory, as long as the correct value of Δt is used.

4. Simulation results and analysis

Very good simulation is achieved for all the measurements using U_c, ρ_0 and j_{c0} as parameters. In figure 1(*a*) the simulation curves of the data presented here are drawn with continuous lines and one of these sets, the set at $T = 50$ K and $H_{ext} = 80$ G, is shown in more detail in figure 2. In the latter it is seen that the magnetic moment initially rises in absolute value (line passing from point A of the curve) as the field is rising. This starting part of the magnetic moment, while the field is ramping, cannot be measured with our commercial SQUID, where data collection starts as soon as the field has reached its final value. However, we will show below that by theoretical estimates we can evaluate the expected experimental values by using the measurements obtained for large times. The maximum, absolute, value of the magnetic moment is reached (point B of the curve in figure 2) when the current becomes as large as the critical current j_c everywhere in the film and cannot rise further (critical state). When subsequently the increase $\dot{H}_a$ stops, the current is lowered immediately (point C of the curve) because, as equation (A15) states, $\dot{g}_K$ will become positive in the absence of $-\dot{H}_a(t)$. The relaxation that follows depends basically on the values of the pinning potential U_c and the critical current j_c. Below we will also present plots of the local magnetic moment and the z component of the magnetic induction on the film surface at the points A, B and C of this measurement as computed by the simulation.

The values of the simulation parameters for all measurements are given in table 1. We find that a strong mutual dependence exists between the parameters ρ_0 and j_{c0}. Generally, all the parameters are related to each other, but each one is basically responsible for a separate characteristic of the relaxation curve. More specifically, ρ_0 determines the maximum value of the magnetic moment during the measurement, U_c determines the slope of the curve at large times (which is almost constant, i.e. m varies almost linearly with $\log t$) and j_{c0} is responsible for the exact level of the line at large times.

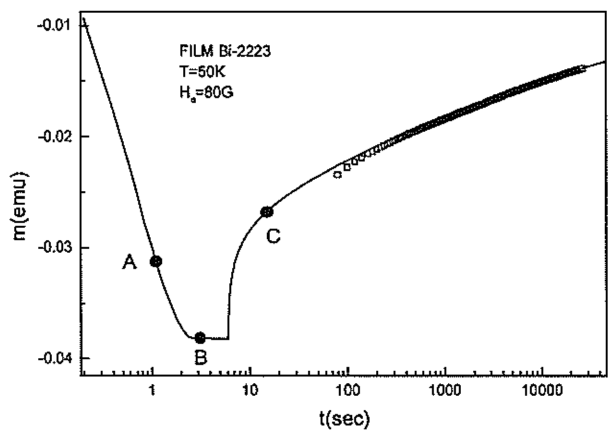

Figure 2. Magnetic relaxation data for the $Bi_2Sr_2Ca_2Cu_3O_8$ thin film taken at temperature $T = 30$ K and applied magnetic field $H_\alpha = 80$ G and the corresponding relaxation curve enlarged.

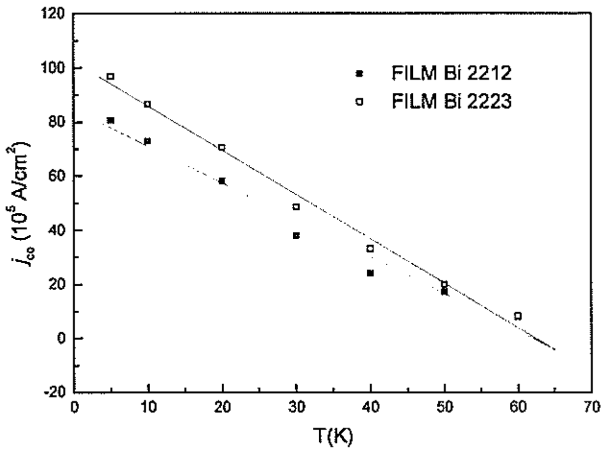

Figure 3. Critical current density j_{c0} of $Bi_2Sr_2CaCu_2O_6$ and $Bi_2Sr_2Ca_2Cu_3O_8$ films at the various temperatures as resulting from the simulation. The lines are guides for the eye.

The maximum, absolute, value of the magnetic moment in the starting part of the curve (point B of figure 2) and also the rate of change of the magnetic moment while the field is ramping depend strongly, as we find from the simulations, on the resistivity ρ_0 and, of course, on the increase rate $\dot{H}_a(t)$ of the field, the latter being fixed by the experiment. Why this is so can be seen from the equation of motion (A15), where the magnitude of $\dot{g}_K(t)$ depends on the value of the difference $c\nabla \cdot [(\rho/d)\nabla g] - \dot{H}_\alpha(t)$: the smaller the value of ρ, the larger the absolute value of this difference (which is negative), the larger the, absolute, rate of change $\dot{g}_K(t)$ and the greater the, absolute, value of the magnetization at the end of the fixed time interval of the field ramping. From the simulations we find that very small values of ρ_0 (e.g. 10^{-11} $\mu\Omega$ cm) result in very large 'diving' of the magnetic moment in this initial stage and in plateau values even 2 orders of magnitude lower than the relaxation part that follows. Still, the rest of the curve can be fitted very well with the experimental data using appropriate values for the parameters U_c, j_{c0}. Since we have no experimental data on this part we have to estimate this maximum value theoretically. A way to do this is provided by the work of Gurevich and Brandt [32], where it is proved that the decay of the magnetic moment is given at large times by

$$m(t) = m(0) + m_1 \ln \tau - m_1 \ln t \tag{4}$$

where

$$\tau = 0.29 \frac{12 m_1}{a^3 \dot{H}_a}. \tag{5}$$

In equations (4) and (5) the initial time $t = 0$ corresponds to the instant when the relaxation starts, i.e. the moment that field ramping is completed, $m(0)$ is the starting value of the relaxation, i.e. the plateau value of figure 2, H_α (G) is the applied field, $m(t)$ (emu) is the magnetic moment of the film at time t, α (cm) its average radius, m_1 (emu) is a parameter connected with the characteristics of the superconductor and τ (s) a characteristic time constant. All magnetic moment parameters $m(t)$, $m(0)$, m_1 are negative. The above equations hold provided that the differential conductivity is approximately $\partial j/\partial E \approx j_1/E$, with j_1 = constant. This can be shown to be true in our case, where $E = \rho j = \rho_0 j\, e^{-U(j)/kT} = \rho_0 j (j/j_c)^n$, $n = U_c/kT$, from which one obtains $\partial j/\partial E \approx j_1/E$, where $j_1/j_c/(n+1)\rho_0^{1/n+1}$ = constant, if one uses $n \gg 1$ which can be verified from table 1. The parameter m_1 of equations (4) and (5) is connected with j_1 with the relation $m_1 = \pi a^3 j_1 d/3c$. Using equations (4) and (5) we fit the large times, linear in $\ln t$, part of each relaxation curve and estimate the value of $m(0)$ in each experiment. In table 1 these values $m(0)$ are depicted. Then, in the simulation procedure we vary the parameter ρ_0, so as to give a plateau value of magnetic moment (point B of figure 2) as close as possible to the above-mentioned value $m(0)$. By comparing $m(0)$ from table 1 with the corresponding plateau values of the relaxation curves from figure 1(a), it can be seen that we succeeded very well in obtaining agreement.

In figure 3 the variation of the critical current j_{c0} with temperature is depicted. For both phases, the critical current falls with temperature almost linearly (the lines are guides to the eye). This is also observed by Niderost *et al* [19] in Bi-2212 single crystals up to 20 K, where single-vortex pinning is assumed to extend. We can also see from this figure that the Bi-2223 thin film has a larger critical current than the Bi-2212 film, which we believe has its origin in stronger pinning in the Bi-2223 film. This is due to the lower anisotropy, but also to a probable existence of stacking faults, which are difficult to do without in the Bi-2223 phase, and also to point defects such as oxygen vacancies or interstitials which must exist in our film, judging from its small critical temperature (84 K) compared with the bulk value (110 K).

The activation energy is also computed during the simulation procedure and it is a function of position since it depends on the local current (and also, if $B_0 \neq \infty$ is used, on the critical current which is a function of the local magnetic field). To give an idea of its variation with the current, we compute the mean values of both the quantities

$\langle U \rangle$ and $\langle j \rangle$ on the surface of the films and the result is plotted in figure 4(*a*) (Bi-2212) and figure 4(*b*) (Bi-2223) for all temperatures. The curves occupy different parts of the $\langle j \rangle$-axis, because, as the temperature grows, the critical current falls and the current decreases everywhere in the film. To display the logarithmic dependence of the activation energy on the current over the whole current range, we have to exclude the factors that depend explicitly on the temperature. Since $U(j, T) = U_c(T)\ln[j_c(T)/j]$, we plot in the insets of figure 4 the quantity $\langle U \rangle / U_c - \ln j_c$ as a function of $\langle j \rangle$, revealing the $\ln j$ dependence. This $\ln j$ relation obviously holds for the local $U(r)$–$j(r)$ values, but it is does not hold in principle for the mean values $\langle U \rangle$ and $\langle j \rangle$ over the surface of the film. The values of the parameter U_c for both films at all temperatures are listed in table 1. It can be seen that they are practically constant with temperature, which is expected if we suppose that the temperature is lower than the depinning temperature [21]. Also, all U_c values for the Bi-2223 film are larger than the corresponding values of the Bi-2212 film, which is a second indication of the existence of stronger pinning in the Bi-2223 phase.

Relaxation measurements of the magnetic moment are a powerful tool for the extraction of the current–voltage dependence of superconductors at very low values of the electric field, such that are not accessible with electric measurements. In figure 5 we present the current–voltage characteristics of the two films as derived from the simulation. From the functions of the simulated current and the electric field, the mean values $\langle E \rangle$ and $\langle j \rangle$ over the surface are computed and they are plotted on a double-logarithmic scale. The plots are linear since a power law was used for the resistivity based on equations (1) and (2) of section 3. It is seen that the curves become less steep, i.e. the slope becomes smaller, as we move towards higher temperatures. Indeed, the exponent $n = U_c/kT$ of the current–voltage characteristic becomes smaller when the temperature rises, as can be seen in table 1. Linear $\log E$–$\log j$ curves are found by many authors who extract them directly from raw data taken with different experimental techniques using no assumption for the form of $U(j)$. From sweep-dependent magnetization measurements Karapetrov *et al* [20] derive linear $\log E$–$\log j$ curves for a Bi-2212 thin film, although in a limited range of electric fields. From magnetic relaxation data on a Bi-2212 single crystal Niderost *et al* [19] also extract linear $\log E$–$\log j$ curves in a single-pancake pinning regime which are in very good agreement with our results.

The dependence of the critical current and the activation energy on the magnetic field is investigated with a second set of relaxation measurements performed at the same temperature and different fields. The results of the simulation of data at $T = 5$ K and $500\ \mathrm{G} \le H \le 40$ kG for both films are shown in table 1. In figure 6 we plot the parameter j_{c0} as a function of the field. This appears to be field dependent because, as we have already said, our assumption that $B_0 = \infty$ in equation (3) is equivalent to j_{c0} actually representing the critical current at the experimental magnetic field and not at $H = 0$. The data are fitted with the exponential law $j_c = A\,\mathrm{e}^{-b/b_0}$ with

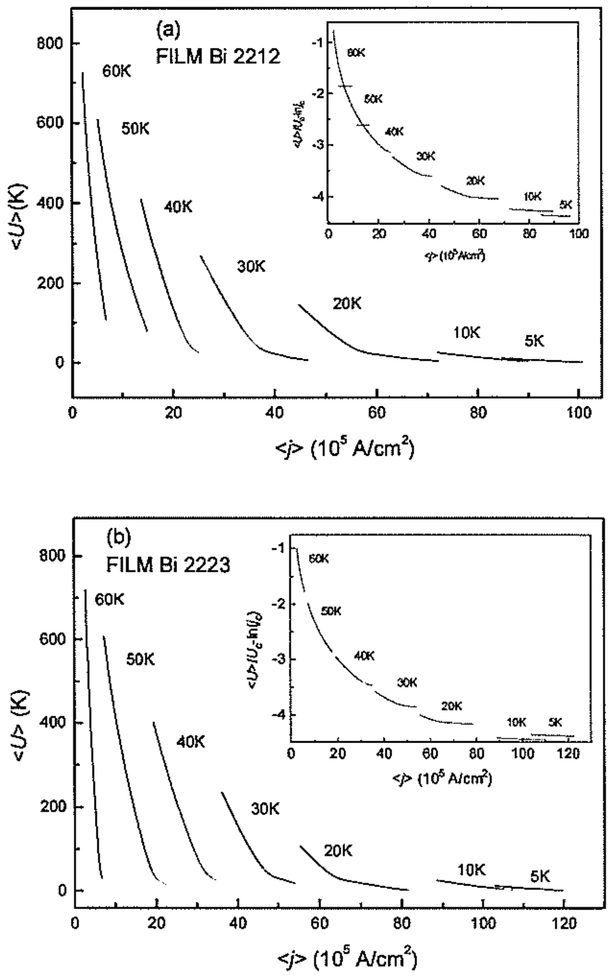

Figure 4. Mean activation energy $\langle U \rangle$ (mean value over the surface) of (*a*) $Bi_2Sr_2CaCu_2O_6$ and (*b*) $Bi_2Sr_2Ca_2Cu_3O_8$ films as a function of the mean current $\langle j \rangle$ (mean value over the surface), both calculated from the simulation. Insets: logarithmic dependence of the temperature-independent quantity $\langle U \rangle / U_c - \ln j_c$ on the mean current $\langle j \rangle$.

$A = 0.8 \times 10^7$ A cm^{-2}, $B_0 = 18\,200$ G for the Bi-2212 film and $A = 1 \times 10^7$ A cm^{-2}, $B_0 = 16\,900$ G for the Bi-2223. This dependence, which is set inactive in the present study, proves to be very appropriate for the investigation of magnetization loops which is actually in progress. From the value of A it is concluded that the critical current density at zero field and temperature $T = 5$ K is 0.8×10^7 A cm^{-2} for the Bi-2212 thin film and 1×10^7 A cm^{-2} for the Bi-2223. Plotting the simulation parameter U_c of the same relaxation data as a function of field (figure 7) we find that it follows a power law $U_c \propto H^{-\alpha}$ with $\alpha = 0.27$ for the Bi-2212 film and $\alpha = 0.30$ for the Bi-2223. Thus the activation energy (2) depends on the magnetic field through both the critical current j_c and the prefactor U_c and it is decreasing with increasing field. This is a rather surprising result since according to the collective-pinning theory U increases with H, while for single-vortex pinning it is almost independent of H. However, Abulafia *et al* [33] have recently found a $B^{-0.7}$ dependence of U close to T_c, and have attributed it to plastic creep of vortices, while H^{-1} predictions have also

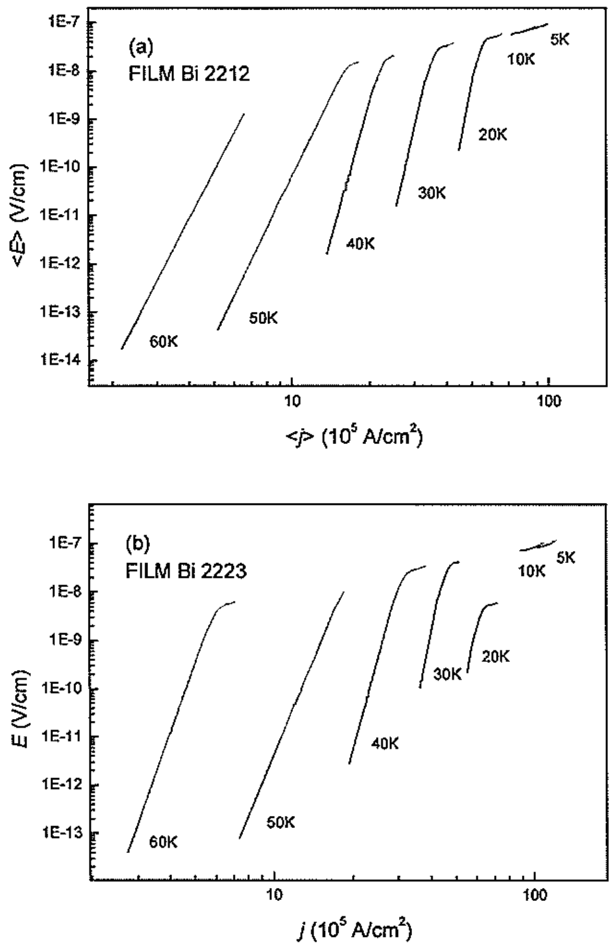

Figure 5. Current–voltage characteristics of (a) $Bi_2Sr_2CaCu_2O_6$ and (b) $Bi_2Sr_2Ca_2Cu_3O_8$ films at various temperatures as calculated from the relaxation.

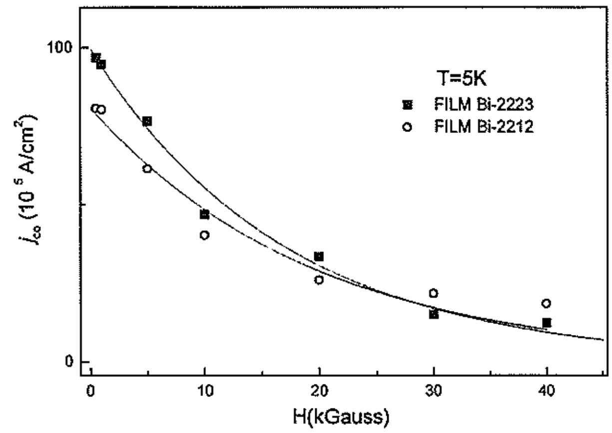

Figure 6. Plot of the parameter j_{c0} as a function of the magnetic field resulting from the simulation of the relaxation measurements at the temperature $T = 5$ K and fields 500 G $\leq H \leq$ 40 kG.

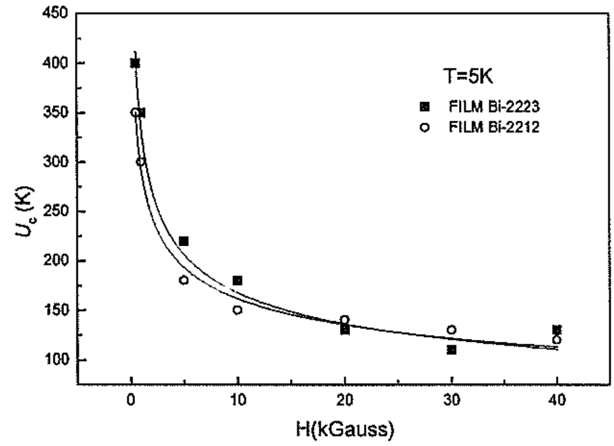

Figure 7. Plot of the parameter U_c as a function of the magnetic field resulting from the simulation of the relaxation measurements at the temperature $T = 5$ K and fields 500 G $\leq H \leq$ 40 kG.

been reported [34–36]. In our case, although the inverse dependence of U on H is unquestionable, we feel that further investigation would be necessary in order to give a definite interpretation of this result.

A remarkable advantage of simulation procedures is that they offer the ability to compute the local variation of the various physical quantities involved. In figure 8 surface plots of the calculated local magnetic moment g (equation (A14)) and in figure 9 contour plots of the z component of the magnetic induction B_z (equation (A7)) are shown at different instants during the experiment. The plots correspond to the points A, B and C of the simulation curve of the Bi-2223 film at temperature 50 K, which was presented in figure 2. At the initial stage of magnetization (point A of figure 2) the local magnetic moment g is still small (figure 8(a)) and varies smoothly over the surface. As one moves towards the centre of the film, more current loops contribute to the magnetization, which is why g increases. At point B of the relaxation curve the currents cannot rise further and the magnetic moment reaches its maximum value. Notice in figure 8(b) that g is not only greater but also steeper, i.e. $\nabla \times zg$ is larger corresponding to larger current, as equation (A5) states. After relaxation has begun (point C of the relaxation curve) the currents decrease and so does the associated magnetic moment (figure 8(c)). The magnetic field plots of figure 9 show that during the increase of H_α (figure 9(a)) shielding is successful in most of the film, but at the edges the magnetic field is not zero owing to demagnetizing effects. Later in the relaxation (figure 9(b)) the magnetic field enters the film almost uniformly and rises slowly (figure 9(c)) as the shielding currents diminish within an unchanged external field.

5. Conclusions

Magnetic relaxation measurements are performed on high-quality $Bi_2Sr_2CaCu_2O_{8+x}$ and $Bi_2Sr_2Ca_2Cu_3O_{10+y}$ thin films at various temperatures from 5 K to 60 K and simulations of them are successfully done. The simulations are based on the numerical integration of the equation of motion for the current of the superconductor, which is derived using the method of Brandt and his coworkers [7–10]. With a thermally activated law assumed

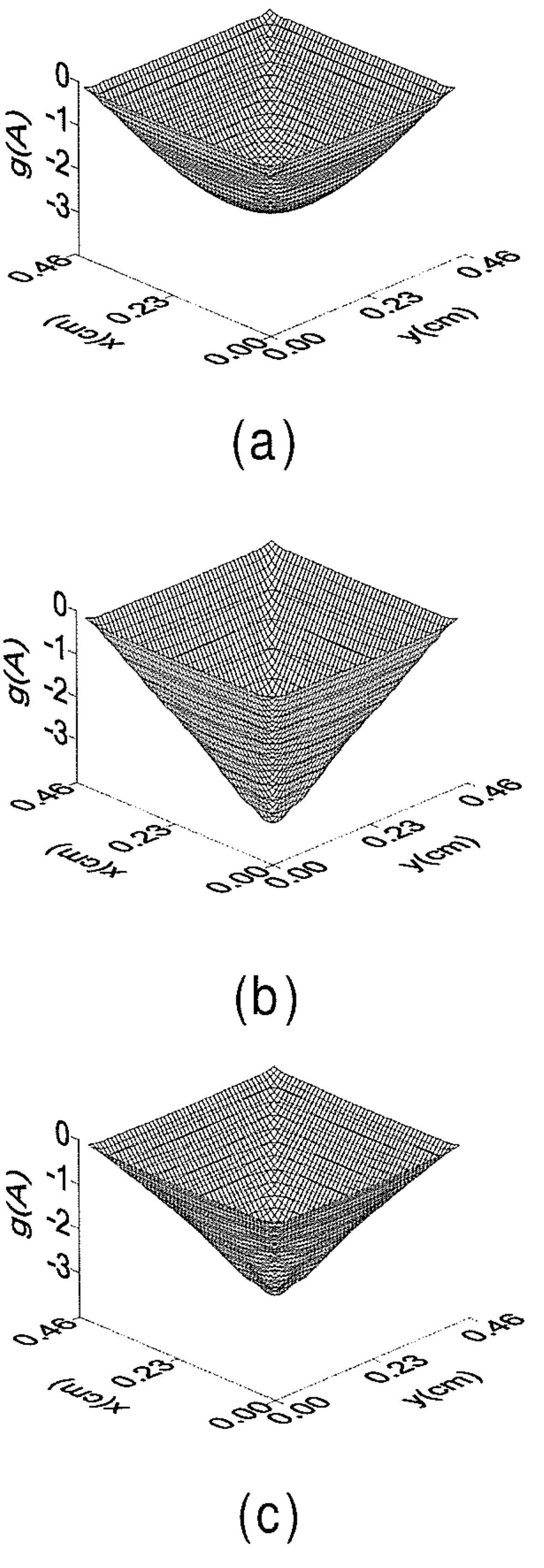

Figure 8. Surface plots of the local magnetic moment g computed by the simulation procedure, as a function of position on the film surface, at the instant corresponding to (*a*) point A, (*b*) point B and (*c*) point C of figure 2.

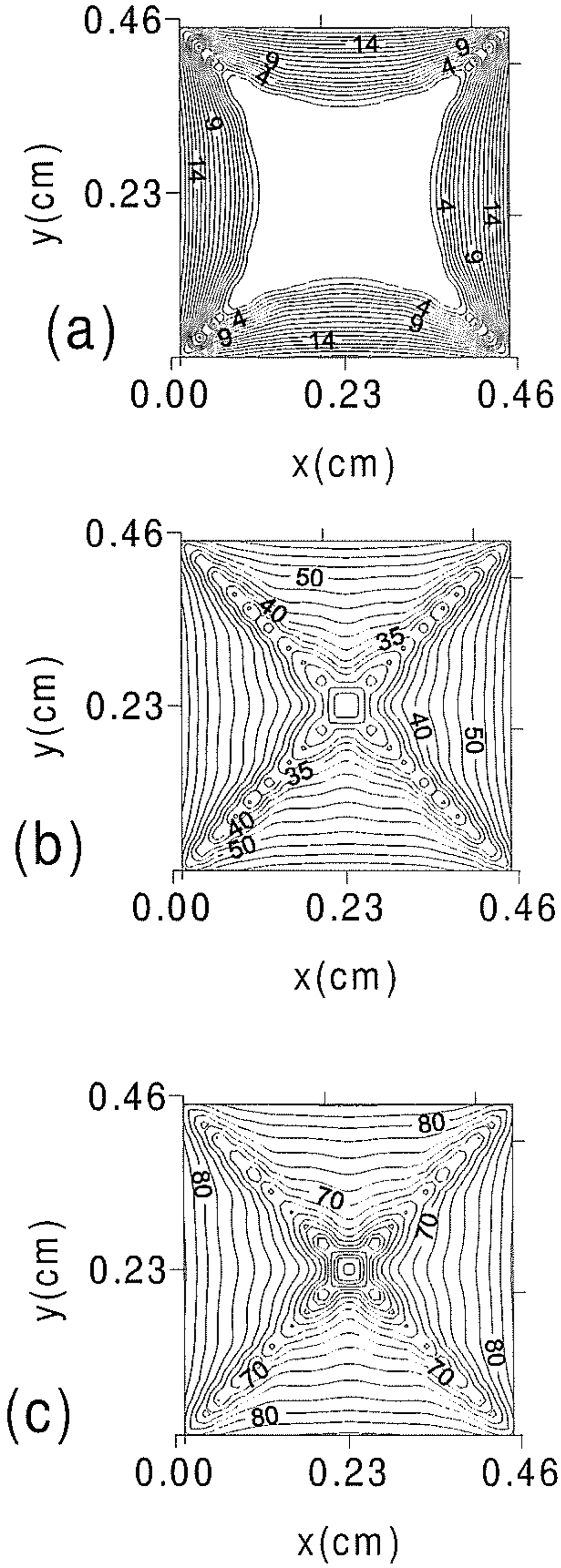

Figure 9. Contour plots of the z component of the magnetic induction B_z calculated from the simulation procedure, as a function of position on the film surface at the instant corresponding to (*a*) point A, (*b*) point B and (*c*) point C of figure 2.

for the resistivity and a logarithmic activation energy the experimental data are fitted successfully for both phases. The critical current is depicted as a function of temperature, decreasing with it linearly, and current–voltage characteristics which are linear on a double-logarithmic scale are derived in an extended current zone. At constant temperature the activation energy is found to decrease with magnetic field according to a power law $B^{-\alpha}$, while the critical current dependence is found to be of the exponential form e^{-B/B_0}. Comparison of the two phases through the simulation parameters and the relaxation rates reveals that pinning in Bi-2223 is stronger, which we attribute to the smaller anisotropy and also to a possible existence of an increased number of defects in this phase.

Appendix

In the following we summarize the theory of a thin rectangular film subject to a magnetic field perpendicular to its surface. The theory has been developed by Brandt and published in several papers [7–9]. We find it useful to summarize this theory here, commenting on a slight modification which we have done to the final equation. We adopt CGS units, which are switched easily to the, closer to experiment, 'practical units', where the constant of light is $c = 10$, the current I is expressed in A, the length x in cm, the magnetic inductance B and magnetic field in G and the magnetic moment m in emu.

Consider an orthogonal parallelepiped superconductor of thickness d and area $2a \times 2b$ subject to an external, homogeneous magnetic field $H_\alpha(t)$ varying with time. Then, an electric field $\boldsymbol{E}(\boldsymbol{r}, t)$ is induced, such that

$$\nabla \times \boldsymbol{E}(\boldsymbol{r}, t) = -\frac{1}{c}\frac{\partial \boldsymbol{B}(\boldsymbol{r}, t)}{\partial t} \quad \text{(A1)}$$

causing a current $\boldsymbol{j}(\boldsymbol{r}, t)$ to flow with value depending on the resistivity $\rho(\boldsymbol{r})$ according to

$$\boldsymbol{E}(\boldsymbol{r}, t) = \rho(\boldsymbol{r})\boldsymbol{j}(\boldsymbol{r}, t). \quad \text{(A2)}$$

We adopt the general case of a spatially varied resistivity, since it must depend on the local magnetic field, which is, according to Biot–Savart's law,

$$\boldsymbol{B}(\boldsymbol{r}, t) = \frac{1}{c}\int_{\substack{volume\\ of\ film}} \frac{\boldsymbol{j} \times (\boldsymbol{r} - \boldsymbol{r}')}{|\boldsymbol{r} - \boldsymbol{r}'|^3}\,\mathrm{d}^3r' + \boldsymbol{H}_\alpha(t). \quad \text{(A3)}$$

It is easy to see that if one differentiates equation (A3) with respect to time and substitutes in it $\boldsymbol{B}(\boldsymbol{r}, t)$ from equation (A1), with $\boldsymbol{E}(\boldsymbol{r}, t)$ substituted by its equivalent from equation (A2), then one has an equation of motion for the current $\boldsymbol{j}(\boldsymbol{r}, t)$ which, if solved, will allow the calculation of all the other electromagnetic quantities.

That is indeed the aim, only first one has to get rid of the coordinate which is normal to the film surface, since its thickness is $d \ll a$. Supposing that the current is independent of z (the x–y plane is taken to coincide with the surface of the film), the 'sheet current' $\boldsymbol{J}(x, y, t)$ is introduced, such that

$$\boldsymbol{J}(x, y, t) = \int_0^d \boldsymbol{j}(x, y, z, t)\,\mathrm{d}z = \boldsymbol{j}(x, y, t)d. \quad \text{(A4)}$$

Furthermore, since the sheet current has to satisfy $\nabla \cdot \boldsymbol{J} = 0$ and also to be parallel to the surface and independent of z, it turns out that it has to depend on a scalar function $g(x, y, t)$ according to the relation

$$\boldsymbol{J}(x, y, t) = \nabla \times \boldsymbol{z}g(x, y, t). \quad \text{(A5)}$$

This z independence that we have assumed actually implies that surface Meissner currents are neglected. This is correct: because of the large demagnetizing factor of the films, the first critical field H_{c1} is very small (some tenths of a gauss), and the Meissner surface currents contribute very little to the magnetic shielding, which is almost entirely successful through the diamagnetic current that results from the gradient of vortices in the film.

Now the current everywhere has to be replaced by its equivalent from equation (A5) and thus equation (A3) gives for the z component of the magnetic field

$$\begin{aligned} B_z(x, y, z, t) &= \iint_{\substack{surface\\ of\ film}} \frac{1}{c}\frac{2z^2 - (x - x')^2 - (y - y')^2}{[z^2 - (x - x')^2 - (y - y')^2]^{5/2}} \\ &\quad \times g(x', y', t)\,\mathrm{d}x'\,\mathrm{d}y' + H_\alpha(t). \end{aligned} \quad \text{(A6)}$$

(A perpendicular external magnetic field has been assumed and the integration for $\mathrm{d}z'$ has been performed.) One last difficulty occurs on taking the limit $\lim_{z\to 0} B_z(x, y, z, t)$ to obtain the magnetic field on the film surface:

$$B_z(x, y, t) = \iint_{\substack{surface\\ of\ film}} Q(\boldsymbol{r}, \boldsymbol{r}')g(x', y', t)\,\mathrm{d}x'\,\mathrm{d}y' + H_\alpha(t) \quad \text{(A7)}$$

where

$$Q(\boldsymbol{r}, \boldsymbol{r}') = \lim_{z\to 0}\frac{1}{c}\frac{2z^2 - (x - x')^2 - (y - y')^2}{[z^2 - (x - x'^2) - (y - y')^2]^{5/2}}. \quad \text{(A8)}$$

$Q(\boldsymbol{r}, \boldsymbol{r}')$ is the so-called integral kernel. However, one cannot directly take the above limit because the remaining integral in equation (A7) diverges. Still, one finds, after long calculations in which a second transformation is inserted, that the Fourier transform of

$$\frac{1}{c}\frac{2z^2 - (x - x')^2 - (y - y')^2}{[z^2 - (x - x'^2) - (y - y')^2]^{5/2}}$$

converges at the limit $z \to 0$ and it is equal to

$$\begin{aligned} Q_{KK'} &= \frac{8}{\pi ab}\frac{1}{c}\int_0^\infty \mathrm{d}q_x \int_0^\infty \mathrm{d}q_y \frac{K_x K'_x(1 + \cos 2aq_x)}{(q_x^2 - K_x^2)(q_x^2 - K_x'^2)} \\ &\quad \times q\frac{K_y K'_y(1 + \cos 2bq_y)}{(q_y^2 - K_y^2)(q_y^2 - K_y'^2)} \end{aligned} \quad \text{(A9)}$$

where $q = (q_x^2 + q_y^2)^{1/2}$ and $Q_{KK'}$ satisfies

$$\begin{aligned} Q(\boldsymbol{r}, \boldsymbol{r}') &= \sum_K \sum_{K'} Q_{KK'}\left(\frac{1}{ab}\right)^{1/2} \sin(K_x x)\sin(K_y y) \\ &\quad \times \left(\frac{1}{ab}\right)^{1/2} \sin(K'_x x')\sin(K'_y y'). \end{aligned} \quad \text{(A10)}$$

From now on, $\boldsymbol{r} = (x, y)$, $\boldsymbol{r}' = (x', y')$.

The integral in equation (A9) can be computed analytically and then $Q(r, r')$ is computed from equation (A10). When $Q(r, r')$ is known, one can proceed to the derivation of the equation of motion for the current.

Inverting equation (A7) to solve for $g(r, t)$ one has

$$g(r,t) = \int_{\substack{surface\\ of\ film}} Q^{-1}(r, r')[B_z(r', t) - H_\alpha(t)]\,\mathrm{d}^2r'.$$

where $Q^{-1}(r, r')$ is the inverse kernel. Differentiation with respect to time gives

$$\dot{g}(r,t) = \int_{\substack{surface\\ of\ film}} Q^{-1}(r, r')[\dot{B}_z(r', t) - \dot{H}_\alpha(t)]\,\mathrm{d}^2r'. \qquad \text{(A11)}$$

Now, inserting equations (A2), (A4) and (A5) into equation (A1) one obtains

$$\dot{B}_z(r,t) = c\nabla \cdot \left[\frac{\rho}{d}\nabla g(r,t)\right] \qquad \text{(A12)}$$

and, with that, equation (A11) becomes

$$\dot{g}(r,t) = \int_{\substack{surface\\ of\ film}} Q^{-1}(r, r') \times \left\{c\nabla' \cdot \left[\frac{\rho}{d}\nabla' g(r', t)\right] - \dot{H}_\alpha(t)\right\}\mathrm{d}^2r' \qquad \text{(A13)}$$

which is an equation of motion for $g(r, t)$. If this is solved, the current on the film can be computed from equation (A5), the magnetic field from equation (A7) and the magnetic moment from the equation

$$m(r,t) = \frac{1}{2c}\int_{\substack{surface\\ of\ film}} r \times J(r,t)\,\mathrm{d}^2r = \frac{1}{c}\hat{z}\int_{\substack{surface\\ of\ film}} g(r,t)\,\mathrm{d}^2r. \qquad \text{(A14)}$$

One can see that $g(r, t)$ is the local magnetic moment, since its integral on the film surface equals the magnetic moment of the film.

At this point we differentiate our work from that of Schuster *et al* [8]. We choose not to solve equation (A13) directly for $g(r, t)$ but, instead, we insert in it the Fourier transform $g_K(t)$ of $g(r, t)$ and solve the resulting equation for $g_K(t)$. That is,

$$\dot{g}_K(t) = \iint_{\substack{surface\\ of\ film}} Q^{-1}(r, r')\left(\frac{1}{ab}\right)^{1/2} \sin(K_x x)\sin(K_y y) \times \left\{c\nabla' \cdot \left[\frac{\rho}{d}\nabla' g(r', t)\right] - \dot{H}_\alpha(t)\right\}\mathrm{d}^2r'\,\mathrm{d}^2r \qquad \text{(A15)}$$

where

$$g(r,t) = \sum_K g_K(t)\left(\frac{1}{ab}\right)^{1/2} \sin(K_x x)\sin(K_y y). \qquad \text{(A16)}$$

By doing so, the spatial derivatives in $\nabla' \cdot (\rho\nabla' g)$ are easily computed, as they are simply sums of terms of $g_K(t)$. Equation (A15) is the desired equation of motion.

References

[1] Bean C P 1962 *Phys. Rev. Lett.* **8** 250
Bean C P 1964 *Rev. Mod. Phys.* **36** 31

[2] Sun J Z, Scharen M J, Bourne L C and Schrieffer J R 1991 *Phys. Rev.* B **44** 5275

[3] Mikheenko P N and Kuzovlev Y 1993 *Physica* C **212** 229

[4] Zhu J, Mester J, Lockhart J and Turneaure J 1993 *Physica* C **212** 216

[5] Brandt E 1994 *Phys. Rev.* B **49** 9024

[6] Brandt E 1994 *Phys. Rev.* B **50** 4034

[7] Brandt E 1995 *Phys. Rev. Lett.* **74** 3025

[8] Schuster Th, Kuhn H and Brandt E 1995 *Phys. Rev.* B **52** 10 375

[9] Brandt E 1992 *Phys. Rev.* B **46** 8628

[10] Rhyner J 1993 *Physica* C **212** 292

[11] Holiastou M, Psycharis V, Niarchos D, Haibach P, Frey U and Adrian H 1997 *Supercond. Sci. Technol.* **10** 712

[12] Holiastou M, Poulakis N, Palles D, Liarokapis E, Niarchos D, Frey U and Adrian H 1997 *Physica* C **282–287** 583

[13] Holiastou M *et al* to be published

[14] Anderson P W 1962 *Phys. Rev. Lett.* **9** 309

[15] Anderson P and Kim Y 1964 *Rev. Mod. Phys.* **36** 39

[16] Feigel'man M and Vinokur V 1990 *Phys. Rev.* B **41** 8986

[17] Zeldov E, Amer N, Koren G, Gupta A, Elfresh M and Gambino R 1989 *Appl. Phys. Lett.* **62** 3093

[18] Zeldov E, Amer N, Koren G, Gupta A, Elfresh M and Gambino R 1990 *Appl. Phys. Lett.* **56** 680

[19] Niderost M, Suter A, Visani P, Mota A and Blatter G 1996 *Phys. Rev.* B **53** 9286

[20] Karapetrov G and Tate J 1995 *Phys. Rev.* B **52** 3776

[21] Abulafia Y, Shaulov A, Wolfus Y, Prozorov R, Burlachov L, Yeshurn Y, Majer D, Zeldov E and Vinokur V 1995 *Phys. Rev. Lett.* **75** 2404

[22] Feigel'man M, Geshkenbein V, Larkin A and Vinokur V 1991 *Phys. Rev.* B **63** 2835

[23] Tinkham M 1996 *Introduction to Superconductivity* 2nd edn (New York: McGraw-Hill)

[24] Blatter G, Feigel'man M, Geshkenbein V, Larkin A and Vinokur V 1994 *Rev. Mod. Phys.* **66** 1125

[25] Vinokur V, Kes P and Koshelev A 1990 *Physica* C **168** 29

[26] Kim S and Raffy Z 1995 *Physica* C **244** 78

[27] Wisniewski A, Puzniak R, Baran M and Szymczak H 1992 *Prog. High Temp. Supercond.* **30** 37

[28] Kim Y B, Hempstead C F and Strnad A R 1962 *Phys. Rev. Lett.* **9** 306

[29] Kim Y B, Hempstead C F and Strnad A R 1962 *Phys. Rev.* **129** 528

[30] Moraitakis E, Pissas M and Niarchos D 1995 *Physica* C **241** 63

[31] van der Beek C J, Nieuwenhuys G J and Kes P H 1992 *Physica* C **197** 320

[32] Gurevich A and Brandt E 1994 *Phys. Rev. Lett.* **73** 178

[33] Abulafia Y, Shaulov A, Wolfus Y, Prozorov R, Burlackov L, Yeshurun Y, Maley D, Zeldov E, Wuhl H, Geshkenbein V and Vinokur V 1996 *Phys. Rev. Lett.* **8** 1596

[34] Yeshurun Y and Malozemoff 1988 *Phys. Rev. Lett.* **60** 2202

[35] Tinkham M 1988 *Phys. Rev. Lett.* **61** 1662

[36] Hettinger J, Swanson A, Skocpol W, Brooks J, Gray-Beal J, Mankiewich P, Howard R, Straughn B and Burk-Hart E 1989 *Phys. Rev. Lett.* **62** 2044